IEEJ Journal of Industry Applications
Vol.7 No.5 pp.445–453 DOI: 10.1541/ieejjia.7.445
Translated from IEEJ Transactions on Industry Applications, Vol.138 No.4 pp.273–281

Paper
(Translation of IEEJ Trans. IA)

Novel Criteria for Reluctance Torque Utility of Permanent Magnet Motors

Akeshi Takahashi* Member, Wataru Hatsuse* Member

This paper presents novel criteria for the reluctance torque utility of permanent magnet (PM) motors. The criteria can be quantified by the PM flux linkage Ψ_p of stator phase windings, and current I, as well as the direct- and quadrature-axis inductance L_d and L_q, respectively. Through both theoretical formulae and experiments, it is proved that a motor with large Ψ_p can utilize little reluctance torque even if the salient-pole ratio L_q/L_d is over 2.0. In such a case, the large salient-pole ratio only leads to an increase in iron loss, and hence a decrease in motor efficiency. The proposed criteria help one to understand the properties inherent in each motor, and also indicate that, in the above case, selecting the rotor geometry with less saliency can improve the efficiency. Results are given for two kinds of PM motors; one is a 4-pole Nd-Fe-B magnet motor with $P_N = 0.6\,\mathrm{kW}$, $n_N = 3600\,\mathrm{min}^{-1}$, Y-connection; the other is a 6-pole ferrite-magnet motor with $P_N = 0.2\,\mathrm{kW}$, $n_N = 1080\,\mathrm{min}^{-1}$, Y-connection.

Keywords: PM motor, reluctance torque, salient-pole ratio, inductance

1. Introduction

The use of high-efficiency permanent magnet (PM) motors in a vast range of applications, such as home appliances and automobiles, has been on the rise, owing to the recent drive towards energy conservation to prevent global warming. An Interior Permanent Magnet (IPM) structure with an embedded permanent magnet in the rotor core is a widely used form of PM motor. In the IPM structure, the ratio of the direct inductance L_d to the quadrature inductance L_q, or what is known as the salient-pole ratio, is large, and hence it is thought that the reluctance torque may be utilized in addition to magnet torque. In the present situation, where it is desirable to reduce the amount of magnet used, a rotor structure that is capable of effectively utilizing the reluctance torque has been studied from various aspects [(1)–(14)].

However, there have been reports which claim that reluctance torque could not be utilized even with the use of the IPM structure, that is, even by increasing the salient pole ratio, depending on the application, the output, and the physical structure of the motor [(15)]. This is because the magnitude of the reluctance torque depends not only on the magnitude of the current but also on its relationship with the magnet torque. In other words, assuming that there is a motor whose magnet torque is 100 times larger than the reluctance torque, the magnitude of the reluctance torque remains insignificant, regardless of the increase in the salient-pole ratio. In fact, in such a motor, increasing the salient-pole ratio increases the amount of magnetic flux generated by the q-axis current (referred to as q-axis current flux hereafter), only leading to reactions such as an increase in iron loss and a consequent decrease in efficiency. Although some useful measures to counter this problem have been reported in the past [(15)(16)], the authors have not come across any material that discusses the quantitative criteria for reluctance torque utility. In the present-day motor design, shape optimization is often carried out using finite element magnetic field analysis (FEA) based on a certain initial shape. Where reluctance torque can be utilized, we may focus on the shape that maximizes it, but in other cases, even the optimization of increasing the salient-pole ratio results only in endless calculation time, and it is not possible to obtain a design solution.

To resolve this problem, we have constructed in this paper, a criterion for reluctance torque utility. Based on this criterion, it is possible to have a quantitative understanding of the impact of the physical structure, the output, the difference in magnetic characteristics, etc., of the motor on the torque composition, and we believe that optimum motor design guidelines can be set for each application at the initial stages of design. We also present a method for improving efficiency in cases where utilization of reluctance torque is difficult. Specifically, by decreasing the salient-pole ratio and reducing the q-axis current flux, it is shown that iron loss can be reduced, and efficiency can be improved. The results of the improved design using a neodymium magnet motor and a ferrite magnet motor as well as actual machine verification are then summarized.

2. Theoretical Formula

The generated torque M_e of the PM motor is generally expressed by the following equation.

$$M_e = \frac{3}{2} \cdot p \cdot \{\Psi_p \cdot I_q + (L_q - L_d) \cdot (-I_d) \cdot I_q\} \cdots\cdots \quad (1)$$

Here, p: the number of pole pairs, Ψ_p: flux linkage for one phase of the stator coil by the permanent magnet, I_d, I_q: dq axis current, L_d, L_q: dq axis inductance. I_d, I_q and Ψ_p are

* Research & Development Group, Hitachi, Ltd.
7-1-1, Omika-cho, Hitachi, Ibaraki 319-1292, Japan

peak values and dq axis coordinate transformation was done using relative transformation.

All the physical quantities shown in the Equation (1) can be determined by analysis or by actual measurement. For example, Ψ_p can be obtained by operating the rotor externally, keeping the terminals of the U, V, W phases of the motor open and measuring the phase voltage peak value E_0 or the line voltage peak value $\sqrt{3}E_0$ at that time. In practical terms, it can be calculated by obtaining the angular frequency ω when the rotor is externally driven at the rotation speed N from Equation (2) and substituting it into Equation (3).

$$\omega = 2\pi \cdot \frac{N}{60} \cdot p \cdots\cdots (2)$$

$$\Psi_p = \frac{E_0}{\omega} \cdots\cdots (3)$$

Now, I_d, I_q, L_d, L_q can be calculated from the voltage vector diagram during motor operation as shown in Fig. 1. If the peak phase of Ψ_p is defined as the d axis, the back EMF E_0, which is the time derivative of Ψ_p, occurs on the q axis where the phase advances by 90°. In Fig. 1, R is the phase resistance, φ is the power factor angle (the phase difference between the current vector $\underline{I}$ and the voltage vector $\underline{U}$), β is the current phase angle, and δ is the voltage load angle.

The first term in Equation (1) represents the magnet torque, and the second term represents the reluctance torque. As is apparent from this equation, the reluctance torque is proportional to $L_q - L_d$. Therefore, the salient-pole ratio L_q/L_d or $L_q - L_d$ has been conventionally used as an index representing the magnitude of the reluctance torque. However, the extent to which the reluctance torque contributes to the generated torque M_e is determined by its relationship with the magnet torque. Hence, in addition to the conventional salient-pole ratio, it is necessary to introduce a new physical quantity which can take into account the relative relationship with the magnet torque in the criterion.

Here, as shown in Fig. 2, the magnet torque is theoretically the maximum when the current phase angle $\beta = 0°$, i.e., when $I_q = I$, and this maximum value $M_{p,max}$ is expressed by the following equation using Equation (1).

$$M_{p,\max} = \frac{3}{2} \cdot p \cdot \Psi_p \cdot I \cdots\cdots (4)$$

The reluctance torque, on the other hand, theoretically becomes the maximum when $\beta = 45°$, and its maximum value $M_{r,max}$ can be expressed by the following equation, again from Equation (1).

$$M_{r,\max} = \frac{3}{2} \cdot p \cdot (L_q - L_d) \cdot \left(\frac{I}{\sqrt{2}}\right)^2 \cdots\cdots (5)$$

The ratio of expressions (4) and (5) is nothing but an index representing the magnitude of the reluctance torque, and hence if this ratio is defined as the reluctance torque ratio α, it can be expressed by the following equation.

$$\alpha = \frac{M_{r,\max}}{M_{p,\max}} = \frac{L_q - L_d}{\Psi_p} \cdot \frac{I}{2} \cdots\cdots (6)$$

$\alpha = 0.1$ means that the maximum value of the reluctance torque is 10% with respect to the maximum value of the magnet torque.

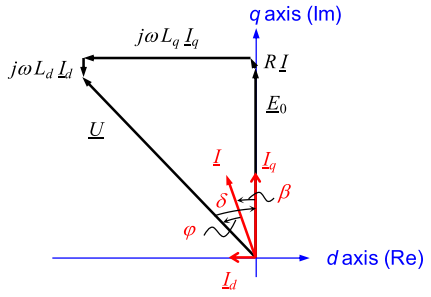

Fig. 1. Vector diagram in motor operation

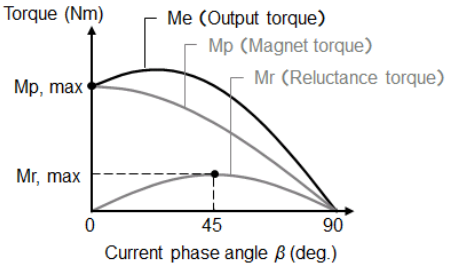

Fig. 2. Characteristics of magnet torque and reluctance torque versus current phase angle

As can be seen from Equation (6), the factors Ψ_p and I have been newly introduced as indexes representing the magnitude of the reluctance torque, in addition to the conventional L_d and L_q. Interestingly, Ψ_p, L_d and L_q are fixed constants for each motor, and we need to determine only I to calculate α. In other words, the magnitude of the reluctance torque can be quantified.

In addition, Equation (6) is consistent with 2 conventionally known facts. The first is the fact that magnet torque becomes dominant when the magnetic flux of the magnet is sufficiently larger than $L_q - L_d$, indicating that there are motors that cannot utilize the reluctance torque in spite of increasing the salient pole ratio or the current. The second is the fact that the reluctance torque ratio α increases as the magnetic flux decreases and approaches the synchronous reluctance motor (SynRM).

In actual operation, owing to the influence of the magnetic saturation due to the application of current, Ψ_p is different from the numerical value obtained in Equation (3) [17]. In this paper, we use Equation (3), laying emphasis on deriving α easily as a criterion at the time of design. For L_d and L_q, we use the numerical value obtained in the energized state when the current phase angle $\beta = 45°$ and when the reluctance torque becomes maximum. The magnitude of the current I is arbitrary, depending on the design point that is being considered. For example, when maximum torque is the focus of the design, maximum current is used, and when rated efficiency is important, rated current is used.

Based on the characteristics shown in Fig. 2, the torque M_e can be expressed by the following equation as a function of $M_{p,max}$, α and β.

$$M_p = M_{p,\max} \cdot \cos\beta \cdots\cdots (7)$$

$$M_r = \alpha \cdot M_{p,\max} \cdot \sin 2\beta \cdots\cdots (8)$$

$$M_e = M_p + M_r = M_{p,\max} \cdot \cos\beta \cdot (1 + 2\alpha \cdot \sin\beta) \cdots\cdots (9)$$

When $dM_e/d\beta = 0$ in Equation (9), the torque M_e becomes maximum. If β at this time is denoted by β_1, the maximum torque $M_{e,\max}$ can be expressed by the following equations.

$$M_{e,\max} = M_{p,\max} \cdot \cos\beta_1 \cdot (1 + 2\alpha \cdot \sin\beta_1) \cdots\cdots (10)$$

$$\sin\beta_1 = \frac{-1 + \sqrt{1 + 32\alpha^2}}{8\alpha} \cdots\cdots (11)$$

$$\cos\beta_1 = \sqrt{1 - \sin^2\beta_1} \cdots\cdots (12)$$

For example, when $\alpha = 0.1$, Equation (10) becomes $M_{e,max} = 1.02M_{p,max}$, and the torque improvement effect due to reluctance torque can be quantified as 2%.

Thus, $M_{e,max}/M_{p,max}$, obtained by modifying Equation (10) itself, represents the torque improvement effect and can be uniquely derived by assigning the reluctance torque ratio α. Figure 3 shows the change in $M_{e,max}/M_{p,max}$ when α is assigned values between 0 and 0.6. From Fig. 3, it can be seen that $M_{e,max}/M_{p,max}$ increases linearly in the region of $\alpha > 0.3$, whereas in the region of $\alpha < 0.3$, it is not affected much by the change in α, and moreover, it is found to be limited to a maximum of about 1.13 pu. In other words, it is difficult to obtain the torque improving effect in the range of $\alpha < 0.3$, even by increasing the reluctance torque ratio α. Furthermore, reactions such as an increase in L_q leading to an increase in iron loss and a consequent decrease in efficiency are significant, as will be described later.

In the foregoing section, we have derived the criteria for reluctance torque utility. In Section 3, we shall describe the comparison with the conventional index using the salient-pole ratio, and application examples of the proposed criteria will be described in Sections 4 and 5.

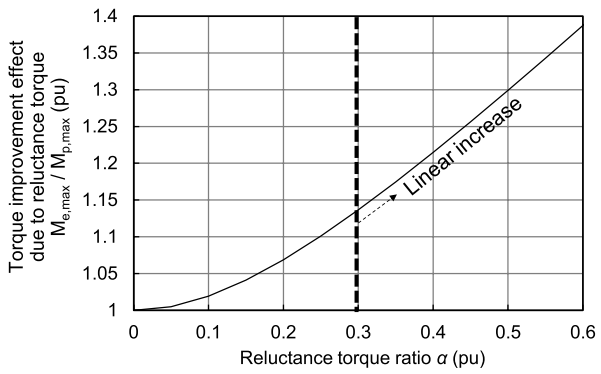

Fig. 3. Relationship between reluctance torque ratio α and torque improvement effect due to reluctance torque $M_{e,\max}/M_{p,\max}$

3. Comparison of Conventional Criteria and the Proposed Criteria

Conventionally, the salient-pole ratio L_q/L_d has been used as an index representing the magnitude of the reluctance torque [(4)–(6)]. However, when comparing motors with different applications, output, and physical structures, conventional indexes often do not work. In the following sections, besides showing concrete examples to prove this point, we also show that the reluctance torque ratio α, derived in Section 2, can be applied across all applications.

Table 1 shows four different types of IPM motors. No.1 is the compressor motor described in Section 4, No.2 is the compressor motor reported in Reference (4) and No.3 and No.4 are the starter generator (SG) and the main motor for the hybrid vehicle (HEV) reported in References (5) and (6) respectively.

Figure 4 shows the relationship between the salient-pole ratio which is a conventional index and the reluctance torque ratio α proposed in this paper. From the Figure, it is evident that there is no correlation between them. As a specific example, No.1 has the largest salient-pole ratio in Table 1, but α is as small as 0.2, indicating that the salient-pole ratio does not function as an index.

We therefore modified Equation (6) as follows, in order to be able to compare motors with different applications, output, and structures in the same dimension. In the following equation, both I and Ψ_p are peak values.

$$\frac{I}{\sqrt{2}} = \alpha \cdot \frac{\sqrt{2}\Psi_p}{L_q - L_d} \cdots\cdots (13)$$

Figure 5 shows the results of plotting the values for motor Nos. 1 to 4 based on Equation (13). Since the left-hand side of Equation (13) is the effective value of the current, this is plotted on the vertical axis of Fig. 5. The term constituted by the motor constants Ψ_p, L_d and L_q is taken as the variable on the horizontal axis, and α is the slope of the linear function. The following conclusions can be made from Fig. 5.

• In the compressor motor, $\sqrt{2}\Psi_p/(L_q - L_d)$ represented by the horizontal axis of Fig. 5 is smaller than that of the HEV motor, but the current ratio on the vertical axis is even smaller. Specifically, the comparison of #1 with #3 shows that the horizontal axis scale ratio is about 1/10, while the vertical axis scale ratio is about 1/30. Hence α becomes smaller

Table 1. Specifications for four types of IPM motors

No.		1	2 [(4)]	3 [(5)]	4 [(6)]
Application		Compressor		SG for HEV	HEV
Output	(kW)	0.6	5	6	50
Magnet arrangement	-	V-shaped	Flat-plate	Flat-plate	V-shaped
Rated current $I/\sqrt{2}$	(A_{rms})	3.50	15	100	188
PM flux linkage Ψ_p	(Wb)	0.111	0.520	0.064	0.200
$(\sqrt{2})\Psi_p / (L_q\text{-}L_d)$	-	17.84	58.32	185.4	279.5
Salient-pole ratio L_q/L_d	(mH)	15.4 / 6.6	23.0 / 12.5	1.76 / 1.27	2.31 / 1.30
	(pu)	2.33	1.84	1.39	1.78
Reluctance torque ratio α	(pu)	0.20	0.26	0.54	0.67

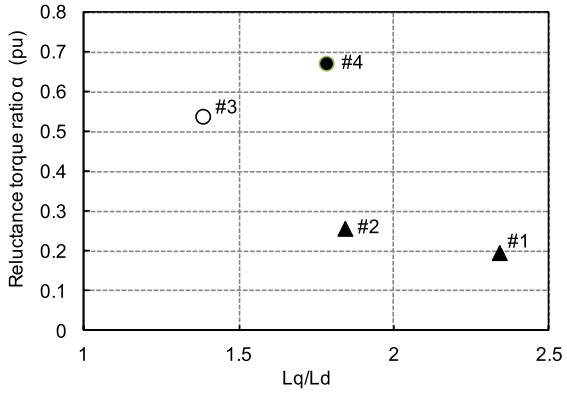

Fig. 4. Relationship between salient-pole ratio and reluctance torque ratio α (#1-4 correspond to those in Table 1)

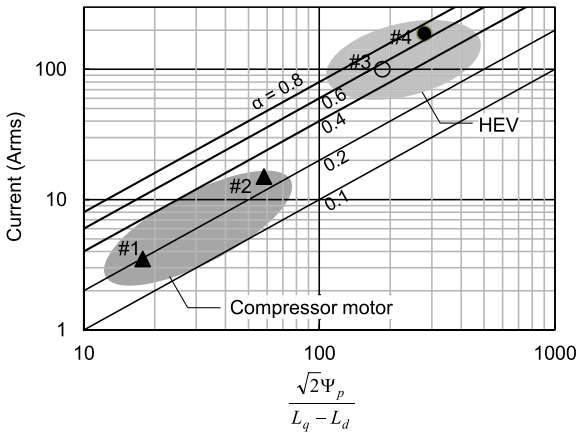

Fig. 5. Correlation of four different types of motors (#1-4 correspond to those in Table 1)

for #1. When α is small as 0.2, it remains at 0.4 even if $L_q - L_d$ is doubled and the maximum torque increase at this time is only 14% (see Fig. 3). That is, the torque increasing effect is remarkably small with respect to the amount of increase of $L_q - L_d$.

• In contrast, in the case of the HEV motor, α tends to increase since the current is large and $L_q - L_d$ is small. When α is as large as 0.6, increasing $L_q - L_d$ by 33% causes α also to increase by 33% to 0.8, and the increase in maximum torque at this time is 13% (see Fig. 3). We may therefore conclude that increasing $L_q - L_d$ tends to contribute to torque increase and improvement of efficiency.

The discussion above shows that the reluctance torque ratio α of the proposed criteria and Equation (13) can be applied to motors with different applications and outputs.

Incidentally, as the design freedom and required torque are different for each of the motors tested, it is not possible to definitively discuss the appropriateness of increasing $L_q - L_d$. However, what is noteworthy is the fact that the introduction of the proposed criterion α makes possible the quantitative evaluation mentioned earlier. Up until now, there was no criteria to judge reluctance torque utility when optimizing the initial shape, and hence, there was no option but to retrospectively interpret the results obtained with FEA. Further, as utilizing reluctance torque was difficult, the only thing to do was to make retrospective judgement from the result of shape optimization. On the contrary, the ratio α proposed in this paper is itself indicative of the magnitude of the reluctance torque and also has the useful functionality of being a criterion for reluctance torque utility in the stage prior to shape optimization with FEA. This will be particularly helpful in quickly drawing up design guidelines that do not rely on reluctance torque when α is small. Through examples of application in real machines in Section 4 and subsequent sections, we shall show that when α is small, iron loss can be reduced and efficiency improved by decreasing the salient-pole ratio and the q-axis current flux.

4. Application Example for Neodymium Magnet Motor

4.1 The Tested Motor Based on the shape shown in Fig. 6(a), we shall attempt to improve the efficiency of the neodymium magnet motor by applying the proposed criterion. The motor is driven by a 3-phase inverter. The specifications are shown in Table 2. The unit notation is used in the discussion that follows, and the reference values of voltage, current, fundamental wave frequency and rated torque are taken to be $\sqrt{2} \cdot U_N = \sqrt{2} \cdot 57.7\,\mathrm{V}$, $\sqrt{2} \cdot I_N = \sqrt{2} \cdot 3.5\,\mathrm{A}$, $f_N = 120\,\mathrm{Hz}$, and $M_N = 1.6\,\mathrm{Nm}$, respectively.

4.2 Analysis result Table 3 shows the motor constants and reluctance torque ratio α. Ψ of the lowermost stage represents the stator flux linkage, which can be calculated as shown below using the motor constants in the table.

$$\Psi = \sqrt{(\Psi_p - L_d \cdot I \cdot \sin\beta_1)^2 + (L_q \cdot I \cdot \cos\beta_1)^2} \quad \cdots\cdots\cdots\cdots\cdots\cdots (14)$$

In model A, one pole is constituted by a permanent magnet arranged in a V shape so that L_q becomes large. Although the salient pole ratio L_q/L_d is as large as 2.33, α being 0.20, the torque improvement effect due to reluctance torque is as small as 7% (see Fig. 3). From Equation (11), the current phase angle β_1 that generates the maximum torque can be calculated as 18.3°, which is far from the current phase angle of 45°, at which the reluctance torque becomes maximum.

Therefore, as shown in model B of Fig. 6(b), one pole was made of a flat plate type permanent magnet so that L_q would be smaller than that of model A. The stator shape was the same for both models A and B. As can be seen in Table 3, L_q/L_d is 1.66, and α is 0.08 in model B, and the torque improvement effect due to reluctance torque disappears, but we believed that this reduction in torque could be offset by reducing the leakage magnetic flux at the ends of the magnet. We also thought that iron loss could be reduced by reducing the q-axis current flux.

Figure 7 shows the loss analysis results under rated conditions (fundamental frequency $f = 1.0\,\mathrm{pu}$, load torque $M_L = 1.0\,\mathrm{pu}$). In model B, iron loss and magnet eddy current loss are both reduced, and the total of the two is 26% smaller than that of model A.

The surface areas of the magnets of models A and B are almost similar, but ribs are arranged in the central portion of the pole in model A, in order to improve the strength. Since ribs are not needed in model B, leakage magnetic flux has decreased, and Ψ_p increased by 5% as a result. As reluctance torque can be compensated by these measures, copper loss

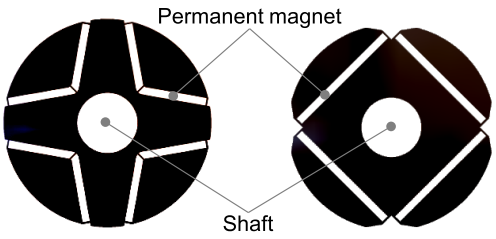

(a) Model A (b) Model B

Fig. 6. Cross section of Nd-Fe-B magnet motors

Table 2. Specifications of Nd-Fe-B magnet motors

Number of pole / slot	4 / 24	-
Winding configuration	distributed	-
PM material	Nd-Fe-B	-
Rated rotation number	3600	(min^{-1})
Outside diameter of stator	112.0	(mm)
Stack length of stator core	35.0	(mm)
Core material	35A300	-
Output power	0.6	(kW)

Table 3. Analysis results of Nd-Fe-B magnet motors

Item		Model A	Model B
Ψ_p	(Wb)	0.111	0.117
I	(A_{rms})	3.5	3.5
L_q / L_d	(mH)	15.4 / 6.6	9.3 / 5.6
	(pu)	2.33	1.66
L_q - L_d	(mH)	8.8	3.7
α	(pu)	0.20	0.08
β_1	(deg.)	18.3	8.6
Ψ	(Wb)	0.124	0.122

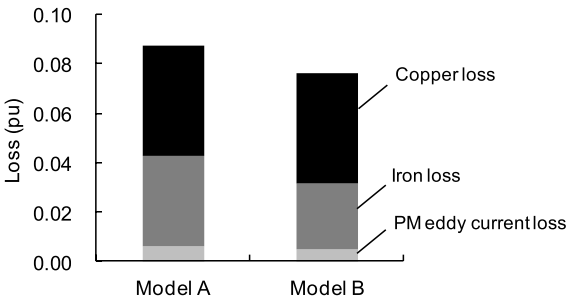

Fig. 7. FEA results of loss (f = 1.0 pu, M_L = 1.0 pu)

may be expected to remain unchanged.

From Table 3, it is seen that there is not much difference in the stator flux linkage Ψ of the two models, and the magnetic flux density level may also be considered to be almost equal. However, these alone cannot explain the reduction in iron loss of model B. We therefore took a closer look at the time variation of the magnetic saturation and the magnetic flux density in the stator, and finally concluded that the main factor of the iron loss reduction in the model B is the reduction of the time harmonic component of the magnetic flux density within the motor due to the reduction of L_q. This mechanism is described in detail below.

Figure 8 is a schematic representation of the magnetic flux density distribution in the machine when q-axis current is applied [18]. The superposition of the magnetic flux of the permanent magnet and the q-axis current flux causes remarkable magnetic saturation of the portions represented by the regions

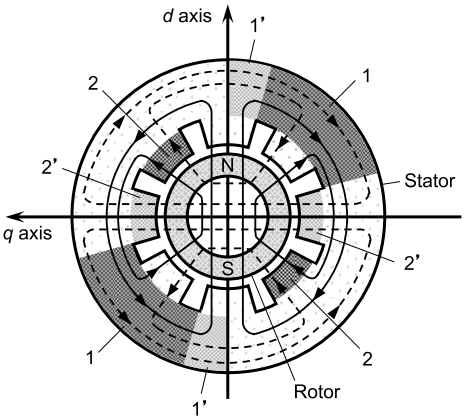

Fig. 8. Schematic of magnetic saturation during I_q operation (solid line: permanent magnet flux, dashed line: flux due to I_q)

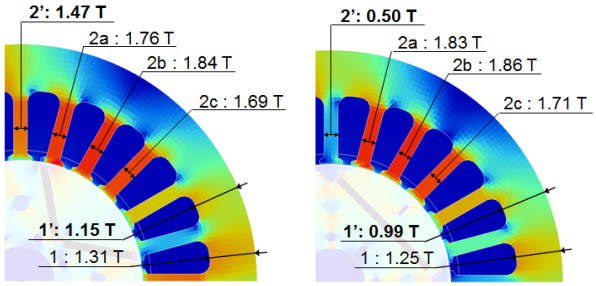

(a) Model A (b) Model B

Fig. 9. FEA results of flux density distribution (f = 1.0 pu, M_L = 1.0 pu)

1 and 2. With the increase in q-axis current flux, the magnetic flux density levels of the regions 1' and 2' increase. The results of visualizing this phenomenon for models A and B are shown in Fig. 9. The portions 1, 1', 2a~2c and 2' correspond to the areas 1, 1', 2 and 2' of Fig. 8. From Fig. 9, we observe that the magnetic flux densities of 1' and 2' in model B are respectively reduced to 86% and 34% with respect to model A. The other parts (1, 2a to 2c) are almost similar. Since the superimposed region of the q-axis current flux is thus reduced, the spatial distribution of the magnetic flux density in the circumferential direction of the stator approaches the sinusoidal wave, the time variation at any point on the stator also becomes sinusoidal, leading to a reduction in iron loss. As a specific example, the time variation of magnetic flux density of the tooth 2c and Fourier series analysis results are shown in Fig. 10. The fundamental wave component is not very different in both models, but the magnetic flux density of model B is low on the whole, and the difference in the 5th, 7th and 9th order components is found to be particularly significant.

The discussion above shows that, even if the magnitudes of the stator linkage flux Ψ are nearly the same in both models, the iron loss varies depending on the superimposed state of the magnetic flux within the motor and that, in model B, the magnetic flux superimposed region is reduced due to the reduction of L_q, leading to the time harmonic component of the magnetic flux density getting lowered and a reduction in iron loss.

4.3 Measurement Results The measurement results of the line-to-line back EMF waveform during no-load

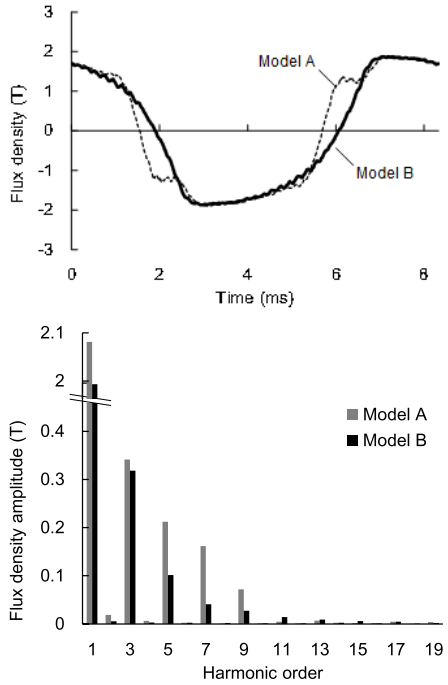

Fig. 10. FEA results of flux density variation at stator teeth in radial direction (f = 1.0 pu, M_L = 1.0 pu)

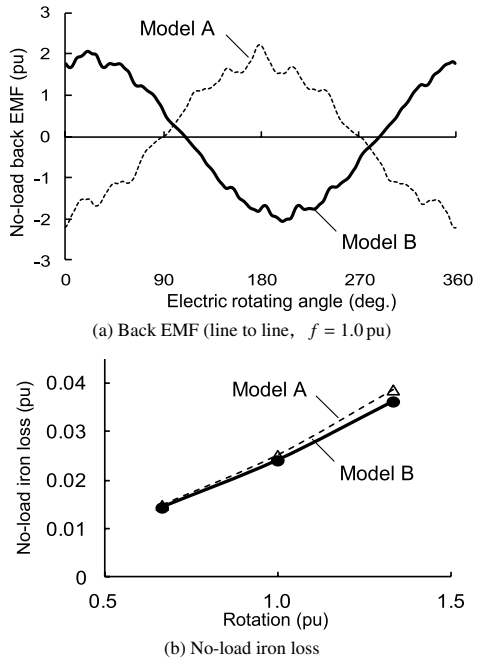

(a) Back EMF (line to line, f = 1.0 pu)

(b) No-load iron loss

Fig. 11. Measured results at no-load external drive

external driving and the no-load iron loss are shown in Fig. 11. Although the back EMF waveforms are slightly different in models A and B, the no-load iron loss is almost the same. It may therefore be concluded that the difference in waveform is unlikely to cause an increase in loss during the operation of the motor.

Figure 12 shows the measurement results at the time of operating the motor. The load torque M_L was 1.0 pu, and the rotation speed was varied between 0.7 and 1.3 pu. The current value was about 1.0 pu in both models. The efficiency of the motor was standardized by taking the efficiency of model A at the rotational speed of 1.0 pu as 100%.

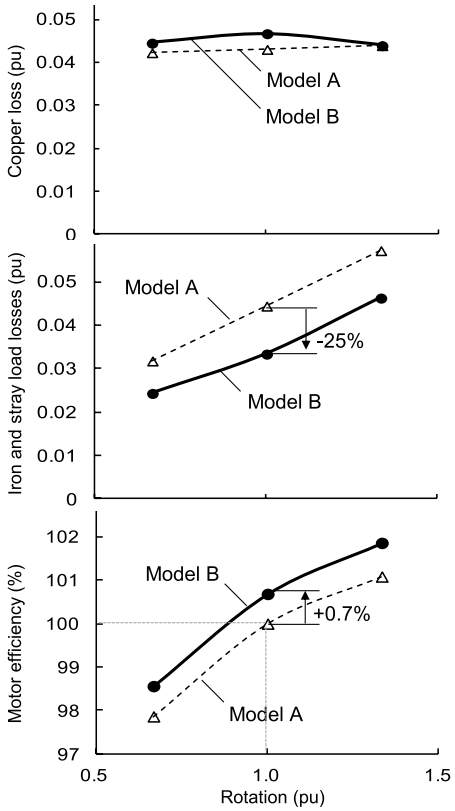

Fig. 12. Measured results at load tests (M_L = 1.0 pu; motor efficiency is normalized setting the rated-rotation efficiency at 100%)

From Fig. 12, it is seen that iron loss and stray loss in model B are reduced by 25% with respect to model A. This is in good agreement with the trend of the analysis result shown in Fig. 7 and validates the fact that by decreasing L_q, the q-axis current flux is reduced, leading to reduction in iron loss. Since there was no significant difference in copper loss, motor efficiency in model B improved by 0.7%.

The discussion above shows that, when the reluctance torque ratio α is about 0.20, as in model A, while the torque improving effect is small, reactions such as increase in iron loss and decrease in efficiency commonly occur, and also that with a structure like model B with reduced L_q, efficiency can be improved without increasing the amount of magnet used.

5. Application Example for Ferrite Magnet Motor

5.1 The Tested Motor The residual magnetic flux density of the ferrite magnet is small, only about 1/3 of the neodymium magnet. In addition, by virtue of its production process, the magnet generally has an arc shape and when made into an IPM structure, it becomes a rotor shape with a large salient-pole ratio, as shown in Fig. 13(a). Therefore, in the ferrite magnet motor, the ratio of the magnet torque is smaller than the neodymium magnet motor, and the ratio of the reluctance torque tends to be large.

Based on the shape shown in Fig. 13(a), we shall attempt to improve the efficiency of the ferrite magnet motor. Although from the qualitative nature of the magnet described above, the principle of actively utilizing the reluctance torque would seem appropriate, it will be shown that in this case also, the

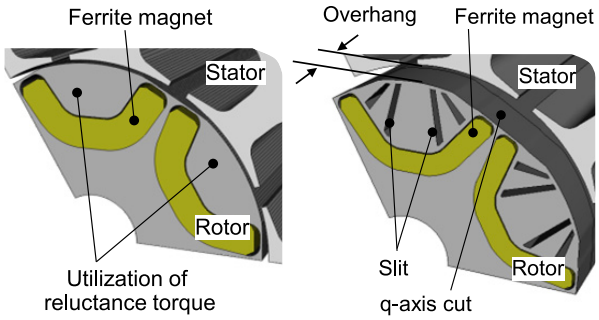

(a) Model X (b) Model Y

Fig. 13. Cross section of ferrite-magnet motors

Table 4. Specifications of ferrite-magnet motors

Number of pole / slot	6 / 9	-
Winding configuration	Concentrated	-
PM material	Ferrite	
Rated rotation number	1080	(min^{-1})
Outside diameter of stator	112.0	(mm)
Stack length of stator core	78.0	(mm)
Core material	35A300	for model X, Y
	35A210	for model Y^+
Output power	0.2	(kW)

Table 5. Analysis results of ferrite-magnet motors

Item		Model X	Model Y
Ψ_p	(Wb)	0.132	0.164
I	(A_{rms})	2.2	2.0
L_q / L_d	(mH)	36.9 / 11.2	12.8 / 8.3
	(pu)	3.29	1.54
L_q - L_d	(mH)	25.7	4.5
α	(pu)	0.30	0.04
β_1	(deg.)	24.0	4.4
Ψ	(Wb)	0.158	0.167

judgment criterion derived in Section 2 is essential. The machine is driven by a 3-phase inverter. The specifications are given in Table 4. The unit notation is used in the discussion that follows, and the reference values of voltage, current, fundamental wave frequency and rated torque are taken to be $\sqrt{2} \cdot U_N = \sqrt{2} \cdot 37.7\,\mathrm{V}$, $\sqrt{2} \cdot I_N = \sqrt{2} \cdot 20\,\mathrm{A}$, $f_N = 54\,\mathrm{Hz}$, and $M_N = 2\,\mathrm{Nm}$, respectively.

5.2 Analysis Result Table 5 shows the motor constants and reluctance torque ratio α. In model X, the salient-pole ratio L_q/L_d is as large as 3.29, but α is 0.30, and the torque improvement effect due to reluctance torque is as small as 13% (see Fig. 3). Hence, it seemed a good idea to apply the principle of increasing the magnet torque without utilizing the reluctance torque. In practical terms, we tried to increase the magnetic flux of the permanent magnet by overhanging the rotor while also reducing L_q as well as effecting iron loss by cutting the rotor core section on the q axis and adding a slit, as shown in Fig. 13(b). This shape is called model Y. Figure 14 shows the relationship between the overhang length on one side and the back EMF. Since the back EMF tends to get saturated even when the overhang is over 10 mm, in the model Y, it was increased by 16% with a 10 mm overhang on one side. In addition, on account of the shape optimization including L_q reduction mentioned above,

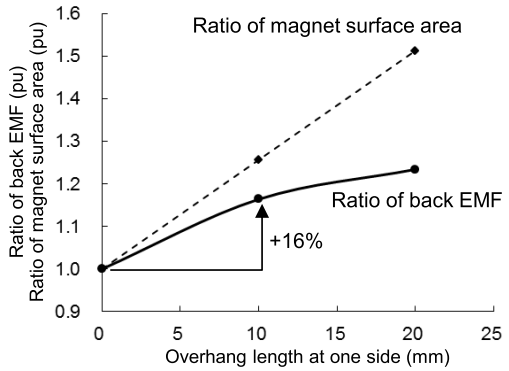

Fig. 14. Overhang length versus ratio of back EMF

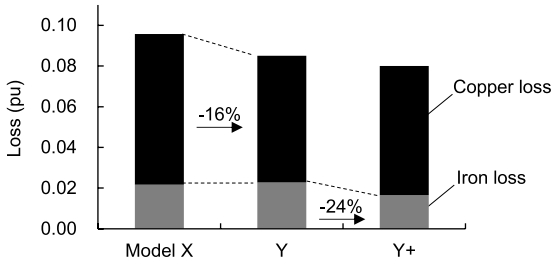

Fig. 15. FEA analysis results of loss ($f = 1.0\,\mathrm{pu}$, $M_L = 1.0\,\mathrm{pu}$)

L_q/L_d became 1.54 and αbecame 0.04. The magnetic flux Ψ_p increased by 25% in the model Y, as shown in Table 5. Therefore, it was estimated that a current reduction of about 10% could be achieved by covering the decrease in reluctance torque with the magnet torque. Since the copper loss varies with the square of the current, it may be expected to reduce by about 20%.

Figure 15 shows the loss analysis results under rated conditions (fundamental frequency $f = 1.0\,\mathrm{pu}$, load torque $M_L = 1.0\,\mathrm{pu}$). Since eddy current loss generated in ferrite magnets can be ignored, the breakdown of copper loss and iron loss has been shown. The copper loss in model Y is reduced and is 16% less than that of model X. The results agree well with the prediction made above. However, the iron loss is nearly the same in both models. In order to further reduce the loss, loss analysis was performed on model Y^+ with electromagnetic steel plate 35 A 210 and the iron loss was found to be 24% less than that of model X.

Despite the 25% increase in magnet flux amount Ψ_p (see Table 5), iron loss in model Y is suppressed to the same level as in model X. The reason for this can be attributed to the fact that the increase in magnetic flux density within the motor can be avoided by reducing L_q. Figure 16 shows the time variation of magnetic flux density and the results of Fourier series analysis of the teeth part. According to the Figure, the magnetic flux densities of the models X and Y are almost equal for both the fundamental wave component and the harmonic wave component. It is also seen from Fig. 16 that the 5^{th}, 7^{th} and 9^{th} harmonic components are negligible, as shown in Section 4, and this is because the peak value of the magnetic flux density is as low as 1.5 T. As described in Section 4, when the magnetic flux density is high, the superimposing region of the q-axis current flux increases with increase in L_q, which is believed to be the reason for the significant increase

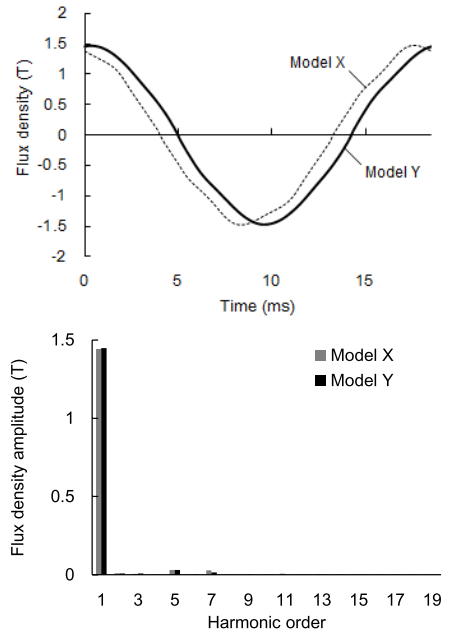

Fig. 16. FEA results of flux density variation at stator teeth in radial direction (f = 1.0 pu, M_L = 1.0 pu)

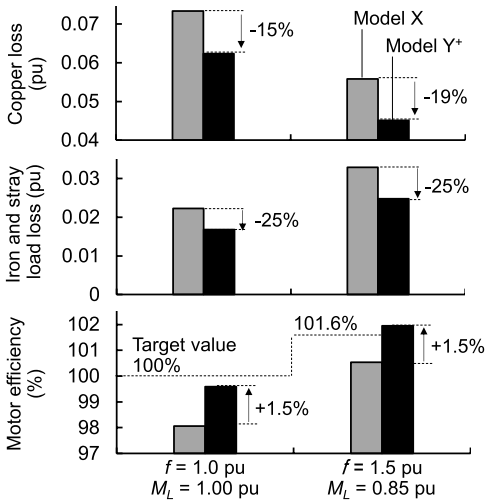

Fig. 17. Measured results at load tests (motor efficiency is normalized setting the rated-rotation efficiency of a Nd-Fe-B magnet motor at 100%)

in the harmonic component of model X.

The discussion above shows that it is possible to suppress the superimposition of the q-axis current flux in model Y by reducing L_q while increasing the magnet flux amount Ψ_p and that increase of iron loss can be suppressed.

5.3 Measurement Result Figure 17 shows the measured results during motor operation. The machines tested were model X and model Y$^+$. Measurements were made under 2 types of conditions: fundamental frequency f = 1.0 pu, load torque M_L = 1.0 pu, and, f = 1.5 pu, M_L = 0.85 pu. The motor efficiency was standardized by taking the rated efficiency of the neodymium magnet motor with the same output as 100%.

From Fig. 17, it is seen that copper loss is reduced by15 to 19% in model Y$^+$ and the current reduction effect due to rotor overhang and shape optimization is also evident. Iron loss has been reduced by 25% and the results also confirm effective suppression of iron loss increase through L_q reduction and effective loss reduction through changing the steel sheet material. The overall result is that the motor efficiency of model Y$^+$ is better than that of model X by 1.5% and that it is almost equal to the target efficiency of the neodymium magnet motor under any operating condition.

These results show that, by using the reluctance torque ratio α proposed in this paper, it is possible to make a quick judgement of reluctance torque utility even for a motor whose salient-pole ratio is large depending on the shape of the ferrite magnet, as in model X. The possibility of deriving a new motor structure like model Y which, while being characterized by L_q reduction, also has improved efficiency has also been shown.

6. Conclusion

The following conclusions have been drawn in this paper.

- The reluctance torque ratio α was derived as a criterion for reluctance torque utility. While the conventional salient pole ratio is not very helpful in clearly judging the utility, it has been shown that the ratioα, derived in this paper, can be used to make such judgments across various types of motors with different applications and outputs.
- In specific terms, the torque improving effect due to reluctance torque is small in the region where $\alpha < 0.3$, but reactions such as increase in iron loss and decrease in efficiency due to superimposition of the q-axis current flux in the stator occur commonly. The results of application in neodymium magnet motor and ferrite magnet motor showed that the derived criterion is suitable and also that improved efficiency can be achieved by adopting a structure with reduced L_q.

References

(1) F. Hetemi, G. Dajaku, and D. Gerling: “Influence of Magnet Thickness and Magnet Orientation on the Performance of IPMSM”, Proc. 19th International Conference on Electrical Machines (ICEM) (2010)

(2) M.E. Hall and J.C. Balda: “Permanent magnet synchronous motor drive for HEV propulsion: optimum speed ratio and parameter determination”, Proc. 56th Vehicular Technology Conference, Vol.3, pp.1500–1504 (2002)

(3) T. Finken and K. Hameyer: “Design and optimization of an IPMSM with fixed outer dimensions for application in HEVs”, Proc. Electric Machines and Drives Conference (IEMDC) ’09, pp.1743–1748 (2009)

(4) A. Takahashi, S. Kikuchi, H. Mikami, K. Ide, and A. Binder: “Reluctance torque utility for line-starting permanent magnet motors”, *IEEE Trans. on Energy Conversion*, Vol.28, No.4, pp.805–814 (2013)

(5) F. Chai, Y. Pei, X. Li, B. Guo, and S. Cheng: “The performance research of starter-generator based on reluctance torque used in HEV”, *IEEE Trans. on Magnetics*, Vol.45, No.1, part 2, pp.635–638 (2009)

(6) C. Ruiwu, C. Mi, and C. Ming: “Quantitative comparison of flux- switching permanent-magnet motors with interior permanent magnet motor for EV, HEV, and PHEV applications”, *IEEE Trans. on Magnetics*, Vol.48, No.8, pp.2374–2384 (2012)

(7) L. Fang and J. Hong: “Flux-barrier design technique for improving torque performance of interior permanent magnet synchronous motor for driving compressor in HEV”, Proc. Vehicle Power and Propulsion Conference (VPPC) ’09, pp.1486–1490 (2009)

(8) P.H. Nguyen, E. Hoang, and M. Gabsi: “Performance synthesis of permanent-magnet synchronous machines during the driving cycle of a hybrid electric vehicle”, *IEEE Trans. on Vehicular Technology*, Vol.60, No.5, pp.1991–1998 (2011)

(9) D.G. Dorrell, A.M. Knight, L. Evans, and M. Popescu: “Analysis and design techniques applied to hybrid vehicle drive machines—assessment of alternative IPM and induction motor topologies”, *IEEE Trans. on Industrial Electronics*, Vol.59, No.10, pp.3690–3699 (2012)

(10) M. Zeraoulia, M.E.H. Benbouzid, and D. Diallo: "Electric motor drive selection issues for HEV propulsion systems: a comparative study", *IEEE Trans. on Vehicular Technology*, Vol.55, No.6 (2006)
(11) K.C. Kim, D.H. Koo, J.P. Hong, and J. Lee: "A study on the characteristics due to pole-arc to pole-pitch ratio and saliency to improve torque performance of IPMSM", *IEEE Transactions on Magnetics*, Vol.43, No.6, pp.2516–2518 (2007)
(12) K.I. Laskaris and A.G. Kladas: "Internal permanent magnet motor design for electric vehicle drive", *IEEE Trans. on Industrial Electronics*, Vol.57, No.1, pp.138–145 (2010)
(13) W. Aimeng, et al.: "Comparison of five topologies for an interior permanent-magnet machine for a hybrid electric vehicle", *IEEE Trans. on Magnetics*, Vol.47, No.10, pp.3606–3609 (2011)
(14) R. Dutta and M.F. Rahman: "Design and analysis of an interior permanent magnet (IPM) machine with very wide constant power operation range", *IEEE Trans. on Energy Conversion*, Vol.23, No.1, pp.25–33 (2008)
(15) H. Koharagi, K. Yamamoto, M. Sasaki, K. Noma, and M. Senoh: "Subjects of small sized permanent magnet motors", The Papers of Tech. Meeting on Rotating Mach., IEE Japan, Vol.RM-04-124 (2004) (in Japanese)
(16) S.A. Evans: "Salient pole shoe shapes of interior permanent magnet synchronous machines", Proc. 19th International Conference on Electrical Machines (ICEM) (2010)
(17) A. Takahashi, S. Kikuchi, S. Wakui, H. Mikami, K. Ide, and K. Shima: "Evaluation of torque characteristics in saturated magnetic field for permanent-magnet synchronous motors", Proc. IEEE Power Engineering Society General Meeting (2007)
(18) A. Takahashi, S. Kikuchi, S. Wakui, H. Mikami, K. Ide, and K. Shima: "Torque characteristics of saturated permanent-magnet synchronous motors", *IEE of Japan*, *Trans.*, Vol.130-D, No.4, pp.492–497 (2010) (in Japanese)

Akeshi Takahashi (Member) (M'08) received a M.Eng. degree from Hokkaido University, Sapporo, Japan, in 2004, and a Dr.-Ing. (Ph.D. equivalent) degree from Darmstadt University of Technology, Darmstadt, Germany, in 2010. From 2004 to 2013, he was with the Hitachi Research Laboratory, Hitachi Ltd., where he conducted research and development of rotating machines. From 2007 to 2008, he was also a visiting researcher at Darmstadt University of Technology. From 2013 to 2016, he was with the Power Systems Business Unit, Hitachi Ltd., where he worked on developing the power supply system for the neutral beam injector of the International Thermonuclear Experimental Reactor (ITER). Since 2016, he has been with the Research & Development Group, Hitachi Ltd., where he is a division leader for motor systems research.

Wataru Hatsuse (Member) received his M.Eng. from Keio University's Graduate School of Science and Technology. He has been with Hitachi, Ltd. since 2007. Currently, he is a researcher with the Hitachi Research Laboratory, where he works on motor drive control.